Supporting Information: Potential and Flux Landscapes Quantify the Stability and Robustness of Budding Yeast Cell Cycle Network

Jin Wang, Chunhe Li, Erkang Wang

March 25, 2010

Methods

Fig. 1 suggests a hypothetical molecular mechanism for budding yeast cell cycle, including DNA synthesis, bud emergence, mitosis, and cell division, which are based on previous investigations.

In this diagram, arrows represent chemical reactions, and box or circle represent concentrations of proteins. Every reaction's rate is determined by the concentrations of related proteins and rate constants. Here, some important reactions rate constants are also labeled. A system state can be specified given all current proteins and their concentrations. Chemical reactions including synthesis, degradation, inactivation, activation, etc, determine how the system state change with time. In this way, a set of differential and algebraic equations could be deduced from the mechanism of Fig.1, based on general principles of biochemical kinetics, which control evolution of system at next moment.

Self Consistent Mean Field Approximation

For monostable state, the steady state probability obtained in the long time limit is around one basin of attraction.

The solution of the equations[1,2,3] determines one of the fixed points and gives the variation around the fixed point, the correspondingly obtained steady state probability is around the fix point or basin of attraction. If the network allows multi-stability, then at every basin of attraction there is a probability distribution centered around it, with different variations. So, the total probability is obtained by summing up all these probability distributions with different weights. The weighting factors $(w_1, w_2, ...)$ represent the size of the basin, which is the relative size among different basin of attraction. For example, $P(x) = w_1 P^a(x) + w_2 P^b(x) + ...$ and $w_1 + w_2 + ... = 1$.

For oscillation, the procedure to obtain probability distribution is different from multi-stable basin. The mean and variances,$\dot{x}(t)$ and $\sigma(t)$, for oscillation are not constants even in steady state, they are functions of time. Here we obtained steady state probability distribution by integration of the probability in time for one period and divide for that

period: $P_{ss} = (\int_{st}^{st+z} P_{oscillation}(x,t)dt)/z$. Here,$z$ is period of oscillation, and st is start point for integration. The same is true how we obtain the steady state probability flux.

Entropy Production Rate

In an non-equilibrium open system, there are constant exchanges in energy and information resulting dissipations. The dissipation of energy, as a global physical characterization of the non-equilibrium system, is closely related to the entropy production rate,in the steady state. The entropy formula for the system is well-known(1),

$$S = -k_B \int P(\mathbf{x},t) \ln P(\mathbf{x},t) dx. \tag{1}$$

By differentiating the above equation, the increase of the entropy at constant temperature T can be obtained as follows:

$$\begin{aligned} T\dot{S} &= k_B * T \int (\ln P + 1) \nabla \cdot \mathbf{J} \, dx \\ &= -\int (k_B T \nabla \ln P - \mathbf{F}) \cdot \mathbf{J} \, dx - \int \mathbf{F} \cdot \mathbf{J} \, dx \end{aligned} \tag{2}$$

where $-\int (k_B T \nabla \ln P - \mathbf{F}) \cdot \mathbf{J} \, dx = e_p$ is the entropy production rate (1), and $\int \mathbf{F} \cdot \mathbf{J} \, dx = h_d$ is the mean rate of the heat dissipation. The $\dot{S} = 0$, in steady state,and the entropy production e_p is equal to the heat dissipation h_d. In this paper, we computed the heat dissipation rate and entropy production at steady state respectively and also verified that they are the same numerically. As we can see, the entropy production rate is the result of combined effects of landscape and flux.

Phase Coherence

The stability of the oscillation with regard to diffusion coefficient D can also be quantified by the phase coherence ξ, which is a measure of the degree of periodicity of the time evolution for a given variable.(2, 3) The phase coherence ξ quantitatively measures the degree of persistence of the oscillatory phase, and is defined as follows: First, the vector $N(t) = n_1(t)e_1 + n_2(t)e_2$ is shown in Fig. S1(A). The unit vectors are $e_1 = (1,0)$ and $e_2 = (0,1)$, $n_1(t)$ and $n_2(t)$ are the concentration of the two kinds of protein molecules at time t. Then $\phi(t)$ is the phase angle between $N(t)$ and $N(t+\tau)$, where τ should be smaller than the deterministic period and larger than the fast fluctuations. We choose $\tau = 2h$. $\phi(t) > 0$ to represent that the oscillation goes on the positive orientation (counterclockwise). The formula of ξ is: $\xi = \frac{2\sum_i \theta(\phi(t))\phi(t)}{\sum_i |\phi(t)|} - 1$, where $\theta(\phi) = 1$ when $\phi(t) > 0$, and $\theta(\phi) = 0$ when $\phi(t) \leqslant 0$, and sums are taken over every time steps for the simulating trajectory. $\xi \approx 0$ implies the system moves stochastically and has no coherence. The oscillation is most coherent when ξ is close to 1.

In the presence of fluctuations, the more periodic the evolution is, the larger the value of ξ is. In Fig. S1(B), ξ decreases when diffusion coefficient D increases, which shows

that larger fluctuations tend to destroy the coherence of the oscillations and therefore the stability of the system.

Flux Integration

The steady state flux can be obtained by taking the long time limit for multi-stable case. For oscillation, we compute flux by integration by time with one period and then divide that period. In equation (3), st is initial time for integration, and z is period, and the variables for integration is x_1(CycB) and x_3(Cdc20).

$$\begin{aligned} J_1(x_1, x_3) &= (\int_{st}^{st+z} J_1(x_1, x_3, t)dt)/z \\ J_3(x_1, x_3) &= (\int_{st}^{st+z} J_3(x_1, x_3, t)dt)/z \end{aligned} \tag{3}$$

Supplementary results

Fig. S2(A)(C) show in the mono-stability regime for 8 variable model, the 2 dimension (in terms of CycB(x_1) and Cdc20(x_3) protein concentration) flux vector and the negative gradient of the potential landscape vector separately with diffusion coefficient D=0.0005, and (B)(D) are directions corresponding to these two vectors. We can see the flux and negative gradient do not share the same direction. Negative gradient points towards the mono-stability basin while the flux flows out of the basin.

Fig. S3(A)(C) show in the bi-stability regime for 8 variable model, the 2 dimension (in terms of CycB(x_1) and Cdc20(x_3) protein concentration) flux vector and the negative gradient of the potential landscape vector separately with diffusion coefficient D=0.0005, and (B)(D) are directions corresponding to these two vectors. We can see again the flux and negative gradient do not share the same direction. Negative gradient points towards the bi-stability basins while the flux spirals out of the basins.

Fig. S4(A)(C) show in the oscillation regime for 8 variable model, the 2 dimension (in terms of CycB(x_1) and Cdc20(x_3) protein concentration) flux vector and the negative gradient of the potential landscape vector separately with diffusion coefficient D=0.0005, and (B)(D) are directions corresponding to these two vectors. From the figure, we can see that the flux vector is obvious at the oscillation path or closed ring, and circulate along the ring. For the force from negative gradient of the potential, they have small magnitude at closed ring, and large magnitude inside and outside the closed ring. In the mean time, their directions are almost vertical to the direction of flux. So, the flux flow and the negative gradient of potential, together as the driven force, form the basic structure of oscillation network.

Fig. S5 show for 8 variable model the change of robustness of network when perturbation level(lp) of chemical reaction rate constants is changed separately for mono-stability, bistable state and oscillation. We can see that with perturbation level increased, RR or barrier height characterizing stability of system, do not increase or decrease monotonously. This observation show that the parameters we choose now are not the

ones that make the system the most stable, and results of entropy production rate in Fig. S5(D)(E) lead to similar conclusion.

Fig. S6 show the distributions of the period and amplitude of oscillations for x_1(CycB) for different fluctuations(SI Appendix). When the fluctuations increase, the distribution of period and amplitude becomes more scattered, and the standard deviation σ of period and amplitude from the mean increases, which means more possible values of the period and amplitude of oscillations can appear. This indicates that less fluctuations corresponding to more stable network make more coherent oscillations with single period and amplitude rather than spread periods and amplitudes.

Fig. S7 show the changes of the barrier height with respect to the changes of the rate constants related with positive feedback loop including $k152, k132, k22, k4, k123$. We can see that when these rate parameters increase, the corresponding barrier height of the landscape increases. This means that the network become more stable, demonstrating that positive feedback loops provide to the network system greater robustness and reliability.

Results of 38 Variables Model

In Fig. S8, we can see the wiring diagram of one complete 38 variables model. Here the basic principle is similar with the 8 variables model, forming bistable state or oscillation in terms of antagonism between Cyclin/CDKs(clb2,clb5) and Enemies(Cdh1/APC,CKI). The START transition is facilitated by SK(cln2), which inactivate Cdh1 and CKI and so make CDKs(clb2,clb5) accumulated, and system enter into S/G2/M state. Once START transition is finished, CDKs are able to suppress CKI by themselves, so SK(cln2) disappear. The FINISH transition is facilitated by EP(exit protein,Cdc20). In S/G2/M, Cdc20 is activated by transcription factor Mcm1, which is activated by Clb2, and Cdc20/APC activate Cdh1 and CKI by making Clbs degraded. System come in to G1 again, and EP(Cdc20) disappear.

Fig. S9(A)(C) show in the mono-stability regime for 38 variable model, the 2 dimension (in terms of Cln2(x_1) and Bud(x_{34}) protein concentration) flux vector and the negative gradient of the potential landscape vector separately with diffusion coefficient D=0.0005, and (B)(D) are directions corresponding to these two vectors. We can see again the flux and negative gradient do not share the same direction. Negative gradient points towards the mono-stability basin while the flux flows out of the basin.

Fig. S10(A)(C) show in the bi-stability regime for 38 variable model, the 2 dimension (in terms of Cln2(x_1) and Bud((x_{34}) protein concentration) flux vector and the negative gradient of the potential landscape vector separately with diffusion coefficient D=0.0005, and (B)(D) are directions corresponding to these two vectors. We can see again the flux and negative gradient do not share the same direction. Negative gradient points towards the bi-stability basins while the flux spirals out of the basins.

Fig. S11(A)(C) show in the oscillation regime for 38 variable model, the 2 dimension (in terms of Cln2(x_1) and Bud(x_{34}) protein concentration) flux vector and the negative gradient of the potential landscape vector separately with diffusion coefficient D=0.0005, and (B)(D) are directions corresponding to these two vectors. From the figure, we can see that the flux vector is obvious at the oscillation path or closed ring, and circulate along the ring. For the force from negative gradient of the potential, they

have small magnitude at closed ring, and large magnitude inside and outside the closed ring. In the mean time, their directions are almost vertical to the direction of flux. So, the flux flow and the negative gradient of potential, together as the driven force, form the basic structure of oscillation network.

So we see very similar global structure of landscapes for budding yeast cell cycle along cell masses with a simplified 8 variable and more sophisticate 38 variable models.

In Fig.S12 we plot the effects of diffusion coefficient D on RR for mono-stability (Fig.S12(A)) and Barrier height for bistable state (Fig.S12(B)) and oscillation (Fig.S12(C)) for 38 variables system. Results show that RR and Barrier height characterizing robustness of system decrease with D increased, and further show that fluctuations decrease stability of system.

We can apply our approach to more detailed model for cell cycle network using 38 protein concentration variables model(4), we can also obtain the potential landscape of this network when the cell mass is changed gradually. Fig.S13 shows the 3 dimension (in terms of Cln2(x_1) and Bud(x_{34}) protein concentration) landscape pictures for D = 0.0005 for 38 variable model.

We can see there are some differences between Fig.S13 and Fig.2 in main text. This is because that at slow growth rates (MDT >= 150 min, corresponding to 8 variable network), newborn cells are smaller than the size at the G1-S transition (m=0.58). Therefore the CDK-controlled system is attracted to the stable G1 steady state, and the cell is waiting until it grows large enough to surpass the transition. Only then can the cell commit to the S/G2/M sequence and the underlying landscape shifts through the transition from bi-stability to oscillation. While at faster growth rates(MDT=90 min, corresponding to 38 variable network), however, newborn cells are already larger than the critical size at the G1-S transition. Therefore they do not linger in a stable G1 state to wait to grow large enough and start the next chromosome.(5) In this condition, network directly enters into oscillation phase seen with large mass as seen in Fig.S13. In the meantime, similar with 8 variables landscape, we can also see that from m=1.1 to m=2.5, the oscillation becomes more and more stable from a series of sequential evolution process just like digging along a ring, two holes, three holes,..., and at last a deep groove.

Mutants

The detailed cell cycle model with 38 variables in Fig.S8 was developed based on the evidences from the phenotypes of many budding yeast mutants(4). These mutants have been constructed by over expressing or deleting each genetic component singly or in multiple combinations. We have investigated 7 mutants that have been used to test the model. For each mutant simulation, we use the same equations and parameter values with wild type, and only change those parameters in terms of mutants.

We also used method of the stochastic Brownian dynamics to study different mutations. We gave a smaller constant, controlling the strength of stochastic fluctuations. Fig.S14 show the stochastic simulation trajectories respectively for mutant1, mutant2,mutant3,and mutant5. From the results, we can see that results from stochastic simulation are close to results of deterministic results, which shows that stochastic simulation and deterministic equations are identical at small fluctuations.

We compared the landscape for wild type and 7 mutations. For wild type, when m=0.5,1.0,1.5,2, we can see that landscape becomes mono-stable, bistable, and oscillation separately.

For mutant1(cdc20(x_{20}) and psd1(x_{31}) are deleted) as shown in Fig.S15 and mutant 3(cdc20($x_2$0) and clb5(x_3) are deleted) (Fig.S17), when m=0.5, mutation makes the system less stable(RR from 1.6 to 1.25). When m=1, network goes from bistable state to mono-stability. When m=1.5 and 2, system goes from oscillation to mono-stability. This is because that Cdc20 initiates the exit from mitosis, deletion of Cdc20 makes that cells not exit from mitosis. So, the landscape keeps the mono-stable shape from m=0.5 to 2.

For mutant2(cdc20(x_{20}),pds1(x_{31}) and clb5(x_3) are deleted) (Fig.S16), when m=2 the barrier height of oscillation decreases from 60 for wild type to 34 for mutant. This shows that model become less stable. When m=1 the barrier height of bi-stability decreases from 245 for wild type to 150 for mutant. When m=0.5 the robustness ratio *RR* of mono-stability decreases from 1.2 for wild type to 1.0 for mutant. From the diagram we know that Pds1 activate PPX by repressing its degradation, and PPX inhibit Cdc14 by activating his opponent Net1. In the mean time, Cdc14 can activate Cdh1. So, the existence of Pds1 make Cdh1 inactive. Additionally, Clb5 is also the enemy of Cdh1. Therefore, the reason of oscillation is rescued might be that deletion of Clb5 and Pds1 together, which both are enemies of Cdh1, are strong enough to activate Cdh1 again. Cdh1 repress Clbs and make system back to G1. So the oscillation is rescued, and system stays in identical phases with the wild type, but less stable.

For mutant5(sic1(x_{10}),cdh1(x_{22}),cdc6(x_5)) (Fig.S18), when m=0.5, mutations make the network more stable(RR from 1.6 to 3.4). When m=1, network goes from bistable state to mono-stable state. When m=1.5 and 2, the network goes from oscillation to mono-stable. This is because that sic1,cdh1 and cdc6 are all enemies of CDK, their deletions make CDK increased and therefore, the network is arrested by telophase. Accordingly, landscape keeps the mono-stable shape from m=0.5 to 2.

For mutant6(cln1,cln2(x_1) and cln3 are deleted) (Fig. S19), when m=0.5, mutations make system more stable(RR from 3.4 to 6.4). When m=1, the network goes from bistable state to mono-stable state. When m=1.5 and 2, system go from oscillation to mono-stable. This is because that cln1,cln2,cln3 phosphorylate and weaken the enemy forces, allowing CDK activity to rise and trigger S phase(6), deletion of cln1,cln2,cln3 makes cells arrest in G1 state. Hence, landscape keeps the mono-stable shape from m=0.5 to 2.

For mutant7(cln1,cln2(x_1),cln3 and cdh1(x_{22}) are deleted) (Fig.S20), when m=0.5, mutations make system less stable(RR from 3.4 to 2.6). When m=1, network goes from bistable state to mono-stable state. When m=1.5 and 2, the network goes from oscillation to mono-stable. The same thing happens with mutant except that cdh1 is deleted. So, network is arrested by mono-stable state for the same reason. In the mean time, compared with mutant6, mono-stable landscape of mutant 7 steps towards the direction of increased CDK. This is reasonable due to the fact that cdh1 deleted is the enemy of CDK.

Discussions

One of the advantages or novelties of this paper is not just constructing the non-equilibrium potential landscape but finding the physical principles and critical roles played by the duality of the potential and flux landscapes for non-equilibrium systems including the biological systems. For real biological systems, such as the budding yeast cell cycle network considered here, the potential landscape drives the system down to the oscillation ring and the flux landscape drives the coherent oscillations on the ring. Without the potential landscape, the system won't be able to reach the oscillation orbit. Without the flux landscape, the system won't be able to circling around to form a coherent oscillation. We absolutely need both for the coherent and stable oscillation of cell cycle. This represents a paradigm shift from the conventional local stability analysis to the global physical approaches with potential and flux in exploring the biological networks.

Furthermore, we developed a self consistent mean field method which allows us to surpass the computational bottleneck of exponential degrees of freedom (reducing it to polynomial number degrees of freedom) and serve as a general framework to explore the underlying potential and flux landscape in multiple dimensions for large realistic biological systems.

Another advantage or novelty of the current approach lies in the following physical pictures from the landscape: The physical pictures of the cell cycle in terms of the change or evolution of the landscape is given: As the mass of the cell increases, the physical process of the cell cycle starts with one basin first formed for G1 stability leading to mono-stability, then another basin emerges for SG2 stability. Furthermore, digging more basins around the ring eventually forms a close circle on the underlying landscape, and the oscillations emerge. We can also explore the transition from one biological phase to another. For example, for the moment (mass=0.58) of transition from G1 to S-G2, the shape of landscape changes accordingly, the second basin of attraction becomes deeper and more stable and G1 looses its stability, so the system begins to enter into S-G2 phase.

It is worthwhile to point out that the origin of the non-zero flux driving the coherent oscillation of cell cycle is the physical energy input in terms of the nutrition supply.

One other novelty of this work is to give a global physical picture, quantify the potential topography and identify a single parameter with the barrier height of the Mexican hat as the stability measure for coherent oscillations of cell cycle. When the height of the Mexican hat is high, the stability and coherent oscillations can be guaranteed. On the other hand, when the height of the Mexican hat is low, the system will loose the stability and coherence of the oscillations will be destroyed.

Therefore, we can study how the barrier height of the Mexican hat varies with different conditions (for network structure and environmental changes) to explore the stability, function and robustness of the cell cycle network. The findings confirm the expectations that fluctuations reduce the stability of the system.

More importantly, we can study how the specific network structures and wirings influence the stability and function of the cell cycle network from landscape point of view. The landscape topography in terms of barrier height can be used to address the global stability and robustness issue which can not be done from other approaches (other

approaches can only address the local stability). Through the changes of the landscape topography (barrier height), we can explore the underlying structures of the network in terms of which specific wirings in the network architecture will be crucial for the global stability and function of the cell cycle process.

For example, from the sensitivity analysis of barrier height changes with respect to different wiring strengths from underlying chemical reaction rates and mutations, we find out the critical wiring links and mutations for the stability and robustness of the cell cycle network, some are consistent with the existing experiments and some are predictions for future experiments to verify. This is not only crucial for identifying the key network structural elements for function but also important for the network engineering and design. This is another novelty of the paper.

8 Variables and 38 Variables Equations

$$
\begin{aligned}
\frac{dm}{dt} &= \mu * (1 - m/mx) \\
\frac{dX_1}{dt} &= k1 - (k21 + k22 * X_2 + k23 * X_4) * X_1 \\
\frac{dX_2}{dt} &= \frac{(k31 + k32 * X_4) * (1 - X_2)}{J3 + 1 - X_2} - \frac{(k4 * m * Cycb + k41 * X_7) * X_2}{J4 + X_2} \\
\frac{dX_3}{dt} &= k51 + k52 * \frac{(m * Cycb)^{nn}}{J5^n n + (m * Cycb)^n n} - k6 * X_3 \\
\frac{dX_4}{dt} &= \frac{k7 * X_5 * (X_3 - X_4)}{J7 + (X_3 - X_4)} - \frac{k8 * Mad * X_4}{J8 + X_4} - k6 * X_4 \\
\frac{dX_5}{dt} &= k9 * m * Cycb * (1 - X_5) - k10 * X_5 \\
\frac{dX_6}{dt} &= k11 - (k121 + k122 * X_7 + k123 * m * Cycb) * X_6 \\
\frac{dX_7}{dt} &= k131 + k132 * X_8 - k14 * X_7 \\
\frac{dX_8}{dt} &= \frac{(k151 * m + k152 * X_7) * (1 - X_8)}{J15 + 1 - X_8} \\
&\quad - \frac{(k161 + k162 * m * Cycb) * X_8}{J16 + X_8}
\end{aligned}
\tag{4}
$$

$$
\begin{aligned}
BCK2 &= B0 * MASS \\
CLN3 &= C0 * Dn3 * MASS/(Jn3 + Dn3 * MASS) \\
SIC1T &= SIC1 + C2 + C5 + SIC1P + C2P + C5P \\
CDC6T &= CDC6 + F2 + F5 + CDC6P + F2P + F5P \\
RENTP &= CDC14T - RENT - CDC14 \\
NET1P &= NET1T - NET1 - CDC14T + CDC14 \\
PE &= ESP1T - ESP1 \\
Vasbf &= kasbf * (esbfn2 * CLN2 + esbfn3 * (CLN3 + BCK2) + esbfb5 * CLB5) \\
Vdb2 &= kdb21 + kdb22 * CDH1 + kdb2p * CDC20 Vdb5 = kdb51 + kdb52 * CDC20 \\
Vkpc1 &= kd1c1 + kd2c1 * (ec1n3 * CLN3 + ec1k2 * BCK2 + ec1n2 * CLN2 + \\
&\quad ec1b2 * CLB2 + ec1b5 * CLB5)/(Jd2c1 + SIC1T) \\
Vppc1 &= kppc1 * CDC14 \\
Vkpf6 &= kd1f6 + kd2f6 * (ef6n3 * CLN3 + ef6k2 * BCK2 + ef6n2 * CLN2 + \\
&\quad ef6b2 * CLB2 + ef6b5 * CLB5)/(Jd2f6 + CDC6T) \\
Vppf6 &= kppf6 * CDC14 \\
Vaiep &= kaiep * CLB2 \\
Vacdh &= kacdh1 + kacdh2 * CDC14 \\
Vicdh &= kicdh1 + kicdh2 * (eicdhn3 * CLN3 + eicdhn2 * CLN2 + eicdhb5 * CLB5 + eicdhb2 * CLB2) \\
Vppnet &= kppnet1 + kppnet2 * PPX \\
Vkpnet &= (kkpnet1 + kkpnet2 * Cdc15) * MASS \\
Vdpds &= kd1pds1 + kd2pds2 * CDC20 + kd3pds2 * CDH1 \\
Vdppx &= kdppx1 + kdppx2 * (J20ppx + CDC20) * Jpds/(Jpds + PDS1) \\
BB(Va, Vi, Ja, Ji) &= Vi - Va + Ja * Vi + Ji * Va \\
GK(Va, Vi, Ja, Ji) &= 2 * Ji * Va/(BB(Va, Vi, Ja, Ji) + \\
&\quad Sqrt(BB(Va, Vi, Ja, Ji)^2 - 4 * (Vi - Va) * Ji * Va)) \\
SBF &= GK(Vasbf, kisbf1 + kisbf2 * CLB2, Jasbf, Jisbf); \\
MCM1 &= GK(kamcm * CLB2, kimcm, Jamcm, Jimcm)
\end{aligned} \tag{5}
$$

$$
\begin{aligned}
\frac{dMASS}{dt} &= kg * MASS \\
\frac{dX_1}{dt} &= (ksn21 + ksn22 * SBF) * MASS - kdn2 * CLN2 \\
\frac{dX_2}{dt} &= (ksb21 + ksb22 * MCM1) * MASS + (kd3c1 * C2P + kd3f6 * F2P) \\
&\quad + (kdib2 * C2 + kdif2 * F2) - (Vdb2 + kasb2 * SIC1 + kasf2 * CDC6) * CLB2 \\
\frac{dX_3}{dt} &= (ksb51 + ksb52 * SBF) * MASS + (kd3c1 * C5P + kd3f6 * F5P) \\
&\quad + (kdib5 * C5 + kdif5 * F5) - (Vdb5 + kasb5 * SIC1 + kasf5 * CDC6) * CLB5 \\
\frac{dX_4}{dt} &= (ksc11 + ksc12 * SWI5) + (Vdb2 * C2 + Vdb5 * C5) + (kdib2 * C2 + kdib5 * C5) \\
&\quad + Vppc1 * SIC1P - (kasb2 * CLB2 + kasb5 * CLB5 + Vkpc1) * SIC1 \\
\frac{dX_5}{dt} &= (ksf61 + ksf62 * SWI5 + ksf621 * SBF) + (Vdb2 * F2 + Vdb5 * F5) \\
&\quad + (kdif2 * F2 + kdif5 * F5) + Vppf6 * CDC6P - (kasf2 * CLB2 + kasf5 * CLB5 + Vkpf6) * CDC6 \\
\frac{dX_6}{dt} &= kasb2 * CLB2 * SIC1 + Vppc1 * C2P - (kdib2 + Vdb2 + \\
&\quad Vkpc1) * C2 \\
\frac{dX_7}{dt} &= kasb5 * CLB5 * SIC1 + Vppc1 * C5P - (kdib5 + Vdb5 + \\
&\quad Vkpc1) * C5 \\
\frac{dX_8}{dt} &= kasf2 * CLB2 * CDC6 + Vppf6 * F2P - (kdif2 + Vdb2 + \\
&\quad Vkpf6) * F2 \\
\frac{dX_9}{dt} &= kasf5 * CLB5 * CDC6 + Vppf6 * F5P - (kdif5 + Vdb5 + \\
&\quad Vkpf6) * F5 \\
\frac{dX_{10}}{dt} &= Vkpc1 * SIC1 - (Vppc1 + kd3c1) * SIC1P + Vdb2 * C2P + \\
&\quad Vdb5 * C5P \\
\frac{dX_{11}}{dt} &= Vkpc1 * C2 - (Vppc1 + kd3c1 + Vdb2) * C2P \\
\frac{dX_{12}}{dt} &= Vkpc1 * C5 - (Vppc1 + kd3c1 + Vdb5) * C5P \\
\frac{dX_{13}}{dt} &= Vkpf6 * CDC6 - (Vppf6 + kd3f6) * CDC6P + Vdb2 * F2P + \\
&\quad Vdb5 * F5P \\
\frac{dX_{14}}{dt} &= Vkpf6 * F2 - (Vppf6 + kd3f6 + Vdb2) * F2P \\
\frac{dX_{15}}{dt} &= Vkpf6 * F5 - (Vppf6 + kd3f6 + Vdb5) * F5P \\
\frac{dX_{16}}{dt} &= ksswi1 + ksswi2 * MCM1 - kdswi * SWI5T \\
\frac{dX_{17}}{dt} &= ksswi1 + ksswi2 * MCM1 + \\
&\quad kaswi * CDC14 * (SWI5T - SWI5) - (kiswi * CLB2 + kdswi) * SWI5 \\
\frac{dX_{18}}{dt} &= Vaiep * (1 - IEP)/(Jaiep + 1 - IEP) - \\
&\quad kiiep * IEP/(Jiiep + IEP) \\
\frac{dX_{19}}{dt} &= (ks201 + ks202 * MCM1) - kd20 * CDC20T \\
\frac{dX_{20}}{dt} &= (ka201 + ka202 * IEP) * (CDC20T - CDC20) - (Vi20 + \\
&\quad kd20) * CDC20
\end{aligned}
$$

$$
\begin{aligned}
\frac{dX_{21}}{dt} &= kscdh - kdcdh * CDH1T \\
\frac{dX_{22}}{dt} &= kscdh - kdcdh * CDH1 + Vacdh * (CDH1T - CDH1)/(Jacdh + CDH1T - CDH1) - \\
&\quad Vicdh * CDH1/(Jicdh + CDH1) \\
\frac{dX_{23}}{dt} &= ks14 - kd14 * CDC14T \\
\frac{dX_{24}}{dt} &= (kdirent * RENT + kdirentp * RENTP) - (kasrent * NET1 + kasrentp * NET1P) * CDC14 \\
&\quad + ks14 - kd14 * CDC14 + kdnet * (RENT + RENTP) \\
\frac{dX_{25}}{dt} &= ksnet - kdnet * NET1T \\
\frac{dX_{26}}{dt} &= kdirent * RENT - kasrent * NET1 * CDC14 + Vppnet * NET1P \\
&\quad - Vkpnet * NET1 + ksnet - kdnet * NET1 + kd14 * RENT \\
\frac{dX_{27}}{dt} &= -kdirent * RENT + kasrent * NET1 * CDC14 + \\
&\quad Vppnet * RENTP - Vkpnet * RENT - (kd14 + kdnet) * RENT \\
\frac{dX_{28}}{dt} &= lte1 * (TEM1T - TEM1)/(Jatem + TEM1T - TEM1) - \\
&\quad BUB2 * TEM1/(Jitem + TEM1) \\
\frac{dX_{29}}{dt} &= (ka151 * (TEM1T - TEM1) + ka152 * TEM1 + \\
&\quad ka15p * CDC14) * (Cdc15T - Cdc15) - ki15 * Cdc15 \\
\frac{dX_{30}}{dt} &= ksppx - Vdppx * PPX \\
\frac{dX_{31}}{dt} &= (kspds1 + ks1pds2 * SBF + ks2pds2 * MCM1) + \\
&\quad kdiesp * PE - (Vdpds + kasesp * ESP1) * PDS1 \\
\frac{dX_{32}}{dt} &= -kasesp * PDS1 * ESP1 + (kdiesp + Vdpds) * PE \\
\frac{dX_{33}}{dt} &= ksori * (eorib5 * CLB5 + eorib2 * CLB2) - kdori * ORI \\
\frac{dX_{34}}{dt} &= ksbud * (ebudn2 * CLN2 + ebudn3 * CLN3 + ebudb5 * CLB5) \\
&\quad -kdbud * BUD \\
\frac{dX_{35}}{dt} &= kspn * CLB2/(Jspn + CLB2) - kdspn * SPN \\
\frac{dX_{36}}{dt} &= 0 \\
\frac{dX_{37}}{dt} &= 0 \\
\frac{dX_{38}}{dt} &= 0
\end{aligned}
\tag{6}
$$

Table 1: Variables of 8 variables model

Variables	Proteins
X_1	CycB
X_2	Cdh1
X_3	Cdc20T
X_4	Cdc20A
X_5	IEP
X_6	CKI
X_7	SK
X_8	TF
m	Cell growth

Table 2: Variables of 38 variables model

Variables	Proteins	Variables	Proteins	Variables	Proteins	Variables	Proteins
X_1	CLN2	X_{11}	C2P	X_{21}	CDH1T	X_{31}	PDS1
X_2	CLB2	X_{12}	C5P	X_{22}	CDH1	X_{32}	ESP1
X_3	CLB5	X_{13}	CDC6P	X_{23}	CDC14T	X_{33}	ORI
X_4	SIC1	X_{14}	F2P	X_{24}	CDC14	X_{34}	BUD
X_5	CDC6	X_{15}	F5P	X_{25}	NET1T	X_{35}	SPN
X_6	C2	X_{16}	SWI5T	X_{26}	NET1	X_{36}	Vi20
X_7	C5	X_{17}	SWI5	X_{27}	RENT	X_{37}	lte1
X_8	F2	X_{18}	IEP	X_{28}	TEM1	X_{38}	BUB2
X_9	F5	X_{19}	CDC20T	X_{29}	Cdc15	MASS	Cell growth
X_{10}	SIC1P	X_{20}	CDC20	X_{30}	PPX		

Table 3: Parameter values of 8 variables model

Component	Rate constants(min^{-1})	Dimensionless constants
CycB	k1=0.04,k21=0.04,k22=1,k23=1	$[CycB]_{threshold} = 0.1$
Cdh1	k31=1,k32=10,k41=2,k4=35	J3=0.04,J4=0.04
Cdc20T	k51=0.005,k52=0.2,k6=0.1	J5=0.3,n=4
Cdc20A	k7=1,k8=0.5	J7=0.001,J8=0.001,[Mad]=1
IE	k9=0.1,k10=0.02	
CKI	k11=1,k21=0.2,k122=50,k123=100	Keq=1000
SK	k13=1,k14=1,k151=1.5,k152=0.05,k161=1,k162=3	J15=0.01,J16=0.01
M	$\mu = 0.01$	mx=10

References

[1] Qian H (2001) Mesoscopic nonequilibrium thermodynamics of single macromolecules and dynamic entropy-energy compensation. *Phys Rev E* 65:016102

[2] Yoda M,Ushikubo T,Inoue W, Sasai M (2007) Roles of noise in single and coupled multiple genetic oscillators. *J Chem Phys* 126:115101.

[3] Wang J, Xu L, Wang EK (2008) Potential Landscape and Flux Framework of Non-Equilibrium Networks: Robustness, Dissipation and Coherence of Biochemical Oscillations. *Proc Natl Acad Sci USA* 105:12271-12276.

[4] Chen KC, Calzone L, Csikasz-Nagy A, Cross FR, *et al*. (2004) Integrative analysis of cell cycle control in budding yeast. *Mol Biol Cell* 15:3841¡ª 3862.

[5] Csikasz-Nagy A, Battogtokh D, Chen KC, Novak B, *et al*. (2006) Analysis of a generic model of eukaryotic cell cycle regulation. Biophys. J. 90:4361-4379.

[6] Tyson JJ, and Novak B (2008) Temporal organization of the cell cycle. *Curr Biol* 18:759-768.

Table 4: Parameter values of 38 variables model for wild type

kg=0.007702	ksn21=0	ksn22=0.15	kdn2=0.12	ksb51=0.0008	ksb52=0.005
kdb51=0.01	kdb52=0.16	ksb21=0.001	ksb22=0.04	kdb21=0.003	kdb22=0.4
kdb2p=0.15	ksc11=0.012	ksc12=0.12	kd1c1=0.01	kd2c1=1	kd3c1=1
kppc1=4	ksf61=0.024	ksf62=0.12	ksf63=0.004	kd1f6=0.01	kd2f6=1
kd3f6=1	kppf6=4	kasb5=50	kdib5=0.06	kasf5=0.01	kdif5=0.01
kasb2=50	kdib2=0.05	kasf2=15	kdif2=0.5	ksswi1=0.005	ksswi2=0.08
kdswi=0.08	kaswi=2	kiswi=0.05	kaapc=0.1	kiapc=0.15	ks201=0.006
ks202=0.6	kd20=0.3	ka201=0.05	ka202=0.2	kscdh=0.01	kdcdh=0.01
kacdh1=0.01	kacdh2=0.8	kicdh1=0.001	kicdh=0.08	ks14=0.2	kd14=0.1
ksnet=0.084	kdnet=0.03	ka151=0.002	ka152=1	ka153=0.001	ki15=0.5
kppnet1=0.05	kppnet2=3	kkpnet1=0.01	kkpnet2=0.6	kasrent=200	kasrentp=1
kdirent=1	kdirentp=2	ksppx=0.1	kdppx1=0.17	kdppx2=2	kspds1=0
ks1pds3=0.03	ks2pds2=0.055	kd1pds1=0.01	kd2pds2=0.2	kd3pds3=0.04	kasesp=50
kdiesp=0.5	ksori=2	kdori=0.06	ksbud=0.2	kdbud=0.06	ksspn=0.1
kdspn=0.06	kasbf=0.38	kisbf1=0.6	kisbf2=8	kamcm=1	kimcm=0.15
esbfn2=2	esbfn3=10	esbfb5=2	ec1n3=0.3	ec1n2=0.06	ec1k2=0.03
ec1b5=0.1	ec1b2=0.45	ef6n3=0.3	ef6n2=0.06	ef6k2=0.03	ef6b5=0.1
ef6b2=0.55	ecdhn3=0.25	ecdhn2=0.4	ecdhb5=8	ecdhb2=1.2	eorib5=0.9
eorib2=0.45	ebudn3=0.05	ebudn2=0.25	ebudb5=1	C0=0.4	Dn3=1
B0=0.054	TEM1T=1	Cdc15T=1	Esp1T=1		
Jd2c1=0.05	Jd2f6=0.05	Jaapc=0.1	Jiapc=0.1	Jacdh=0.03	Jicdh=0.03
Jatem=0.1	Jitem=0.1	Jasbf=0.01	Jisbf=0.01	Jamcm=0.1	Jimcm=0.1
Jspn=0.14	Jn3=6	J20ppx=0.15	Jpds=0.04	Kez=0.3	Kez2=0.2
kmad2=8(for [ORI]>1 and [SPN]<1) or 0.01(otherwise)					
kbub2=1(for [ORI]>1 and [SPN]<1) or 0.2 (otherwise)					
kltel=1(for [SPN]>1 and [Clb2]>Kez1) or 0.01 (otherwise)					

Figure

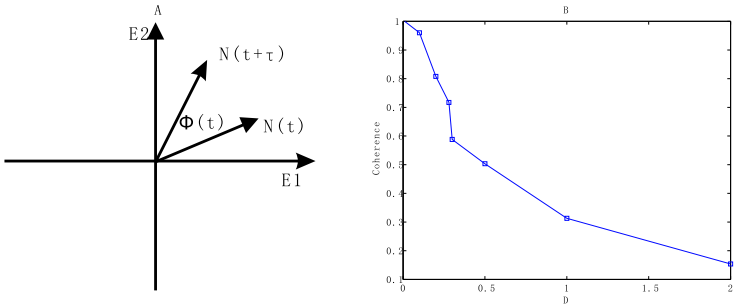

Fig.S 1: (A) shows the definition of phase coherence. (B) shows coherence versus external noise D for oscillation.

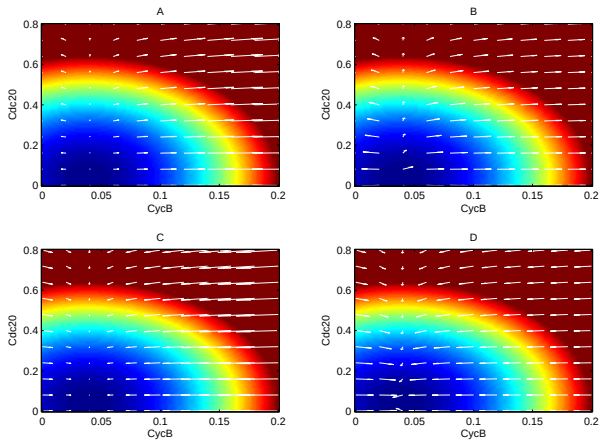

Fig.S 2: Flux and gradient potential force for monostable. Shown are the vector graphs of the flux (A), the force from negative gradient of the energy landscape (C), and the direction of those forces with diffusion coefficient D = 0.0005 (B, D).

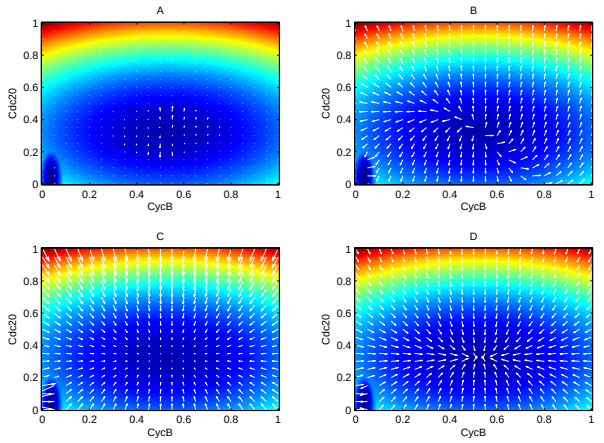

Fig.S 3: Flux and gradient potential force for bistable. Shown are the vector graphs of the flux (A), the force from negative gradient of the energy landscape (C), and the direction of those forces with diffusion coefficient D = 0.0005 (B, D).

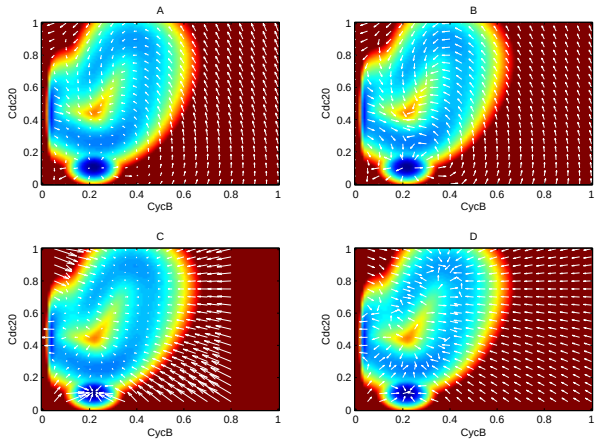

Fig.S 4: Flux and gradient potential force for oscillation. Shown are the vector graphs of the flux (A), the force from negative gradient of the energy landscape (C), and the direction of those forces with diffusion coefficient D = 0.0005 (B, D).

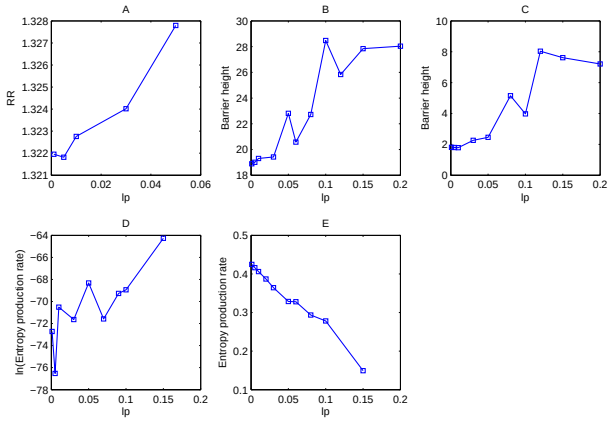

Fig.S 5: (A),(B),(C)show Robustness or barrier height versus perturbation level lp for monostable, bistable, and oscillation separately. (D),(E)show Entropy production rate versus perturbation level lp for monostable, bistable separately.

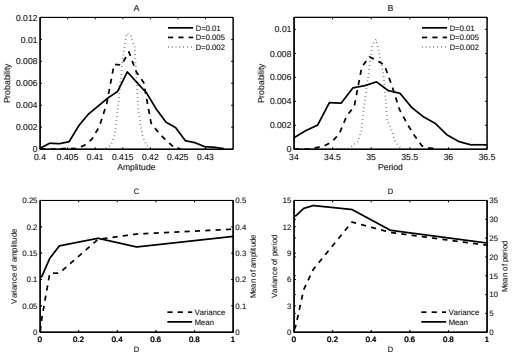

Fig.S 6: (A) show distribution of amplitude, (C) show standard deviation and mean of amplitude versus external noise D for oscillation,(B) show distribution of period, (D) show standard deviation and mean of period versus external noise D for oscillation.

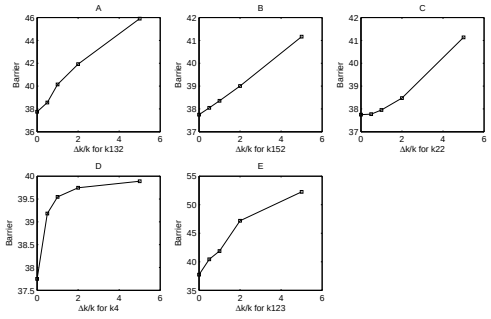

Fig.S 7: (A)(B)(C)(D) (E) show effects of changing rate constants related with positive feedback loop on the barrier height for oscillation. $\Delta k/k$ represents the percent of parameters increased.

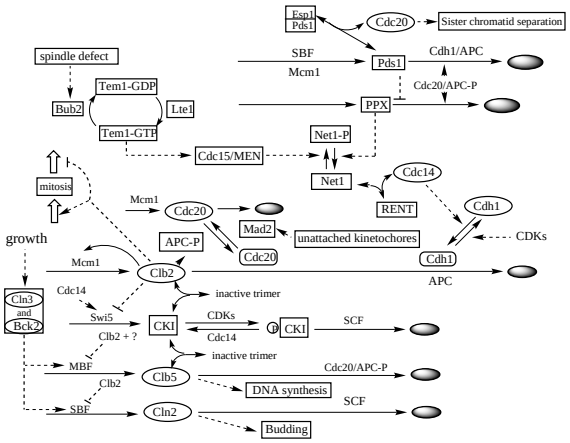

Fig.S 8: The basic cell cycle engine in eukaryotic cells for 38 variables model.

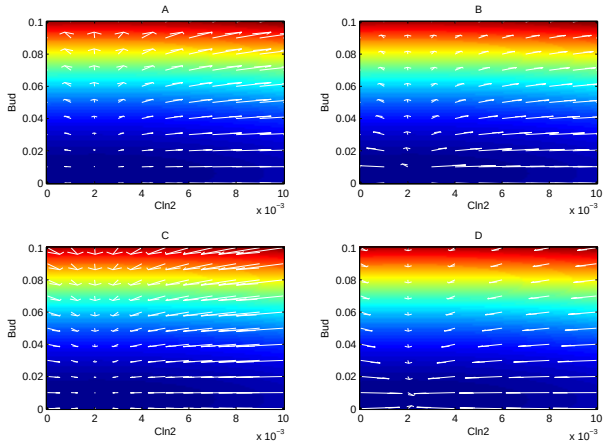

Fig.S 9: Flux and gradient potential force for monostable when m=0.4 for 38 variables model. Shown are the vector graphs of the flux (A), the force from negative gradient of the energy landscape (C), and the direction of those forces with diffusion coefficient D = 0.0005 (B, D).

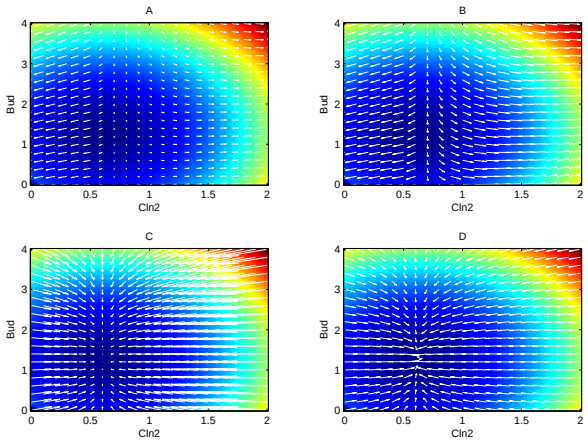

Fig.S 10: Flux and gradient potential force for bistable when m=0.8 for 38 variables model. Shown are the vector graphs of the flux (A), the force from negative gradient of the energy landscape (C), and the direction of those forces with diffusion coefficient D = 0.0005 (B, D).

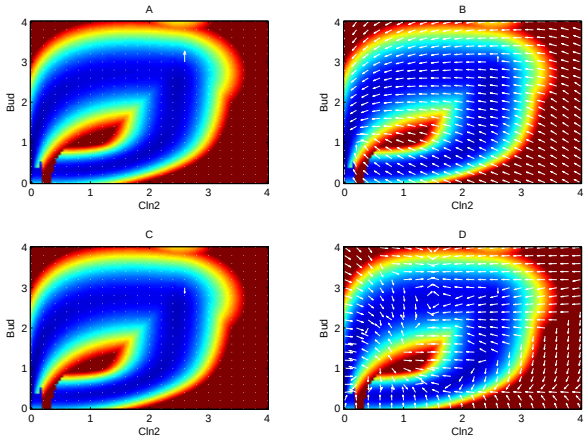

Fig.S 11: Flux and gradient potential force for oscillation when m=2 for 38 variables model. Shown are the vector graphs of the flux (A), the force from negative gradient of the energy landscape (C), and the direction of those forces with diffusion coefficient D = 0.0005 (B, D).

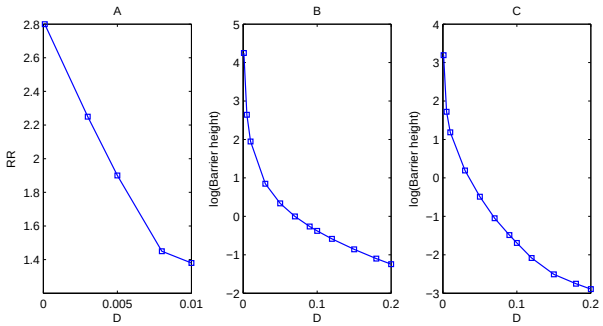

Fig.S 12: (A),(B),(C)show robustness ratio versus diffusion coefficient D for monostability and Barrier height versus diffusion coefficient D for bistable and oscillation separately for 38 variables model.

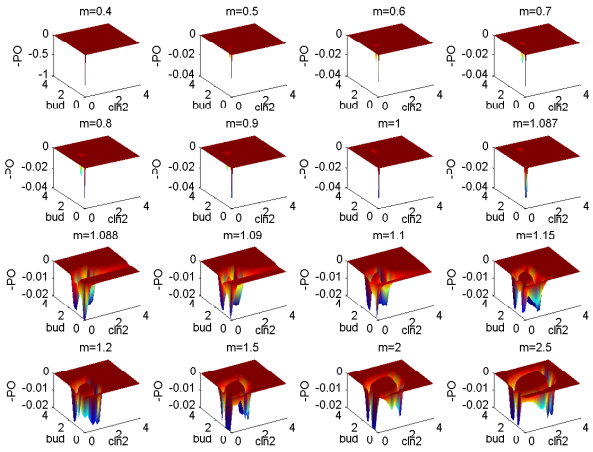

Fig.S 13: Figures show the 3 dimension landscape picture from bistable to oscillation for 38 variables model.

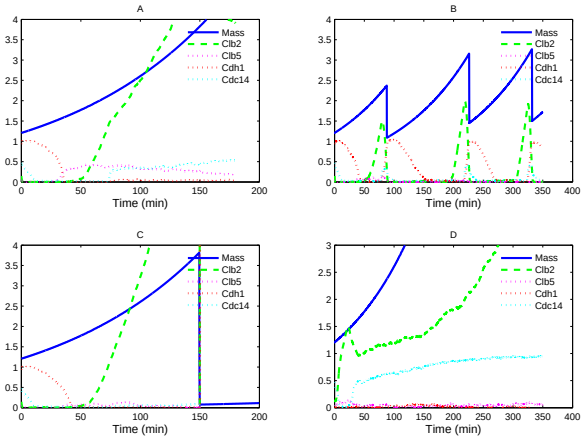

Fig.S 14: Mutations. (A) shows the trajectory of mutant1(cdc20,pds1), (B) shows the trajectory of mutant2(cdc20,pds1,clb5),(C) shows the trajectory of mutant3(cdc20,clb5),(D) shows the trajectory of mutant5(sic1,cdh1,cdc6)

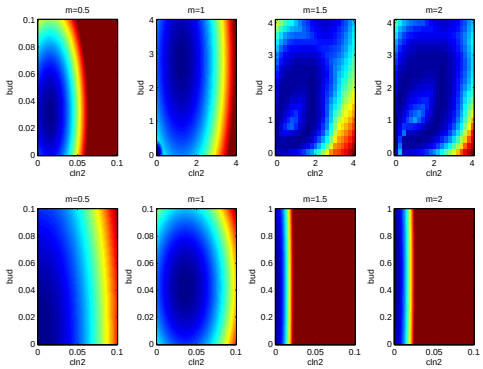

Fig.S 15: Mutations 1:cdc20 pds1. ks201=0,ks202=0,ks1pds2=0,ks2pds2=0

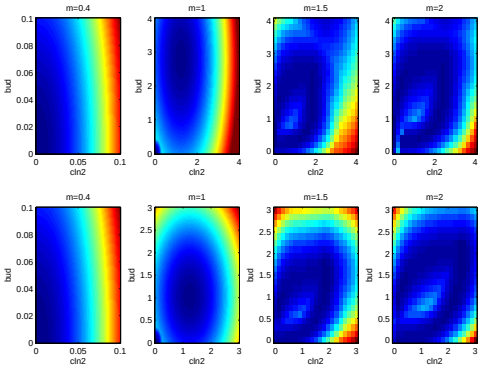

Fig.S 16: Mutation2: cdc20,pds1,clb5. ks201=ks202=0,ksb51=ksb52=0,ks1pds2=ks2pds2=0.

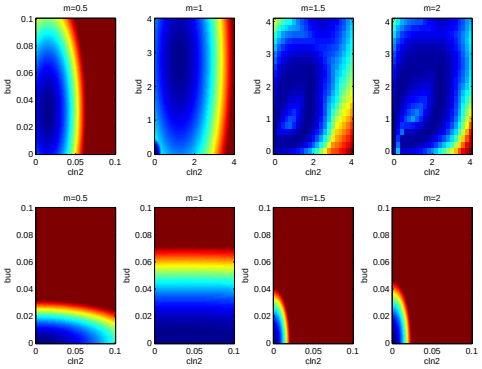

Fig.S 17: Mutation3: cdc20, clb5.ks201=0,ks202=0,ksb51=0,ksb52=0.

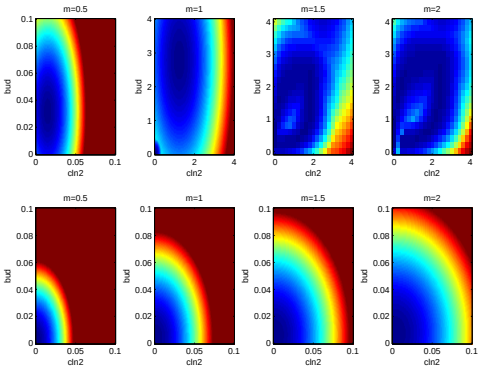

Fig.S 18: Mutation5: sic1,cdh1,cdc6. ksf61=ksf62=ksf63=0,ksc11=ksc12=0,kscdh=0,initial CDH1T=CDH1=0.

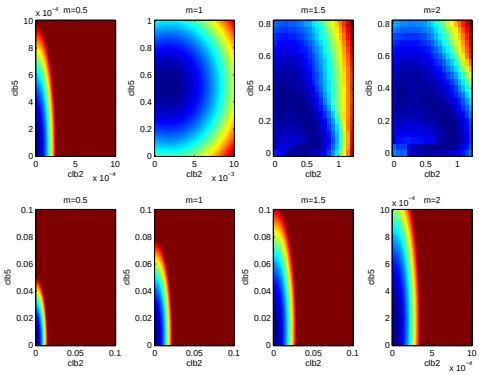

Fig.S 19: Mutation6:cln1,cln2,cln3. ksn21=ksn22=0,Dn3=0.

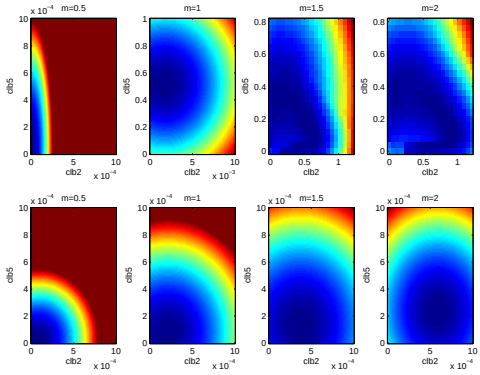

Fig.S 20: Mutation7: cln1,cln2,cln3,cdh1.ksn21=ksn22=0,Dn3=0,kscdh=0,initial CDH1=CDH1T=0.